Connecting Magic Dynamics in Thermofield Double States to Spectral Form Factors

Ning Sun[1] and Pengfei Zhang[1,2,*]
[1]State Key Laboratory of Surface Physics and Department of Physics, Fudan University, Shanghai, 200438, China
[2]Hefei National Laboratory, Hefei 230088, China

(Received 6 February 2026; accepted 12 June 2026; published 13 July 2026)

Under unitary evolution, chaotic quantum systems initialized in simple states rapidly develop high complexity, precluding any efficient classical description. The hardness of classical simulation within the stabilizer formalism, commonly referred to as magic resources, can be quantified by the stabilizer Rényi entropy, while quantum chaos can be characterized by spectral properties of the Hamiltonian, most notably through the spectral form factor. In this Letter, we propose a relation between the dynamics of the stabilizer Rényi entropy for thermofield double states and the spectral form factor, based on general arguments for chaotic systems with all-to-all interactions. This relation implies that the saturation of the stabilizer Rényi entropy is governed by a first-order dynamical transition. We then demonstrate this relation explicitly in the Sachdev-Ye-Kitaev model, using an auxiliary-spin representation of the stabilizer Rényi entropy that exhibits an emergent Z_2 symmetry. We further find that, in the high-temperature regime of the SYK model, the transition occurs at a finite time, with the long-time phase marked by spontaneous Z_2 symmetry breaking. By contrast, at low temperatures, the transition is pushed to times exponentially long in the system size. Our results reveal an intriguing interplay between quantum chaos and magic resources.

DOI: 10.1103/p4s9-9smn

Introduction—While the Hilbert space dimension of quantum systems grows exponentially, certain physically relevant states still admit efficient classical representations. For example, states with low entanglement entropy can be described by tensor network states [1,2], enabling the development of classical algorithms for computing ground-state properties of gapped quantum many-body systems. Another important class of quantum states consists of stabilizer states, which have wide applications in quantum error correction [3]. By the Gottesman-Knill theorem, such states can be efficiently represented within the stabilizer formalism [4–7]. To quantify the nonstabilizerness of a general quantum state, the stabilizer Rényi entropy (SRE) has been introduced [8–13]. Alternative measures of magic resources have also been proposed, including the robustness of magic, Wigner negativity, and mana [14–21].

More recently, considerable attention has been devoted to the study of magic resources in quantum many-body systems, including Hamiltonian systems [22–42], matrix product states [43–46], and dynamics generated by quantum circuits [47–54]. Most of these studies focus on the SRE because of its direct interpretation as an observable in replicated systems, enabling both theoretical and numerical analysis. One fundamental question that we focus on is how the SRE develops and saturates under chaotic Hamiltonian dynamics. In particular, we ask how the growth of magic resources is related to the spectral statistics of the Hamiltonian [55–57], which serve as a diagnostic of quantum chaos. Addressing this question also provides important insight into the growth of complexity in chaotic systems, which underlies quantum thermalization [58–61]. A major obstacle is the intrinsic hardness of classical simulation once the SRE becomes extensive, which prevents the identification of universal relations that emerge in the thermodynamic limit.

In this Letter, we investigate the dynamics of the SRE and establish a direct connection to the spectral form factor (SFF) [56,57,62] by focusing on thermofield double (TFD) states [63,64], which have broad applications in condensed matter physics [65,66], quantum information [67–76], quantum field theory [77–79], and gravitational physics [64]. We first present a general argument for this relation in chaotic systems with all-to-all interactions and then demonstrate it explicitly in the Sachdev-Ye-Kitaev (SYK) model [80–83] using a path-integral approach with auxiliary spins that exhibit an emergent Z_2 symmetry [40]. This relation implies that the saturation of the SRE is accompanied by a first-order dynamical transition, producing a singularity in the SRE. In the SYK model, the short- and long-time dynamics are governed by distinct saddle points. The short-time saddle preserves the Z_2 symmetry, in which the SRE is related to the slope of the SFF, whereas the long-time saddle spontaneously breaks the Z_2 symmetry, yielding a nearly maximal

*Contact author: PengfeiZhang.physics@gmail.com

SRE. At high temperatures, the transition occurs at a finite time; at low temperatures, the transition is controlled by soft modes and occurs only at exponentially long times. Our results uncover a fundamental link between quantum chaos and magic resources.

Setup—We consider systems consisting of N Majorana fermion modes ψ_j that satisfy the canonical anticommutation relations $\{\psi_j, \psi_k\} = \delta_{jk}$. The Hamiltonian H is assumed to be chaotic with all-to-all interactions, exhibiting random-matrix-like behavior in its level statistics [55,56]. A standard diagnostic of quantum chaos is the spectral form factor (SFF) [56,57,62], defined as $\mathrm{SFF}_\beta(t) = |Z(\beta + it)|^2$. Here, $Z(\beta) = \mathrm{tr}(e^{-\beta H})$ denotes the partition function of the thermal density matrix. For chaotic Hamiltonians, the SFF exhibits a characteristic slope-ramp-plateau structure as a function of time. At early times, the SFF shows a rapid decay, which is self-averaged [57]. At intermediate times, the SFF develops a linear ramp, which reflects level repulsion and spectral rigidity captured by random matrix theory. Finally, at late times beyond the Heisenberg time, the SFF saturates to a constant plateau at $Z(2\beta)$, signaling the discreteness of the energy spectrum.

We are interested in the quench dynamics of the system. In particular, we focus on a special class of pure initial states that admit a concrete path-integral representation, namely, TFD states [63,64]. These states are widely used to characterize symmetries of density matrices [65,66] and to perform many-body teleportation protocols [67–76]. To construct the TFD state, we introduce N auxiliary fermion modes ξ_j and define a maximally entangled state by the condition $(\psi_j + i\xi_j)|\mathrm{EPR}\rangle = 0$ for all j. Following the standard terminology, we refer to ψ as the left system and ξ as the right system. The TFD state is then defined as [84]

$$|\mathrm{TFD}\rangle = e^{-\frac{\beta}{2}H}|\mathrm{EPR}\rangle/\sqrt{Z(\beta)}. \tag{1}$$

We initialize the total system with $2N$ Majorana fermions in the TFD state at $t = 0$ and evolve it under the Hamiltonian H. At time t, the density matrix is $\rho(t) = e^{-iHt}|\mathrm{TFD}\rangle\langle\mathrm{TFD}|e^{iHt}$, for which we compute the SRE. In particular, the evolved state with $\beta = 0$ can be viewed as the Choi representation of the unitary operator [85], which has been studied in Ref. [54].

The definition of the SRE in fermionic systems requires introducing an orthonormal operator basis of Majorana strings [24]:

$$\Psi_{\boldsymbol{v}_L,\boldsymbol{v}_R} = i^{\frac{v_t(v_t-1)}{2}} 2^{\frac{v_t}{2}} \psi_1^{v_{L,1}} \ldots \psi_N^{v_{L,N}} \xi_1^{v_{R,1}} \ldots \xi_N^{v_{R,N}}, \tag{2}$$

where we have introduced two N-dimensional vectors $\boldsymbol{v}_L$ and $\boldsymbol{v}_R$, with components $v_{L,j}, v_{R,j} \in \{0,1\}$. The quantity $v_t = |\boldsymbol{v}_L| + |\boldsymbol{v}_R| \equiv \sum_j (v_{L,j} + v_{R,j})$ counts the number of nontrivial Majorana operators, and the coefficients ensure that $\Psi_{\boldsymbol{v}_L,\boldsymbol{v}_R}$ is Hermitian and satisfies $\Psi^2_{\boldsymbol{v}_L,\boldsymbol{v}_R} = 1$. The density matrix can be expanded in this basis as $\rho(t) = (1/2^N)\sum_{\boldsymbol{v}_L,\boldsymbol{v}_R} c_{\boldsymbol{v}_L,\boldsymbol{v}_R}(t)\Psi_{\boldsymbol{v}_L,\boldsymbol{v}_R}$, where $c_{\boldsymbol{v}_L,\boldsymbol{v}_R}(t) = \mathrm{tr}_{LR}[\rho(t)\Psi_{\boldsymbol{v}_L,\boldsymbol{v}_R}]$ is known as the Majorana spectrum [24]. Here, we add a subscript to denote the trace over the total Hilbert space. The Majorana spectrum satisfies the normalization condition $\sum_{\boldsymbol{v}_L,\boldsymbol{v}_R} c_{\boldsymbol{v}_L,\boldsymbol{v}_R}(t)^2 = 2^N$. The SRE is then defined as

$$M_2(t) \equiv -\ln\left(2^{-N}\sum_{\boldsymbol{v}_L,\boldsymbol{v}_R} c_{\boldsymbol{v}_L,\boldsymbol{v}_R}(t)^4\right). \tag{3}$$

It measures the distance between a generic state and the set of stabilizer states. Any pure stabilizer state is a simultaneous eigenstate of 2^N commuting Majorana strings, known as the stabilizers. For these stabilizers, we have $|c_{\boldsymbol{v}_L,\boldsymbol{v}_R}(t)| = 1$ while $|c_{\boldsymbol{v}_L,\boldsymbol{v}_R}(t)| = 0$ for all remaining Majorana strings. An example is the maximally entangled state $|\mathrm{EPR}\rangle$, which is stabilized by 2^N operators satisfying $\boldsymbol{v}_L = \boldsymbol{v}_R$. Consequently, we find $M_2 = 0$ for stabilizer states. For more general states, $M_2(t)$ satisfies the bound $0 \le M_2(t) \le N\ln 2$ [8]. In the following discussion, we focus primarily on the extensive part of the SRE, $\lim_{N\to\infty} M(t)/N$, neglecting subleading corrections arising from finite-size effects.

General argument—We first present a general argument establishing the relation between the SRE and the SFF. Using properties of the EPR state, the Majorana spectrum can be expressed as a Wightman function:

$$c_{\boldsymbol{v}_L,\boldsymbol{v}_R}(t) = \frac{i^{n_{\boldsymbol{v}_L,\boldsymbol{v}_R}}}{Z(\beta)}\mathrm{tr}\left(e^{-\left(\frac{\beta}{2}-it\right)H}\Psi_{\boldsymbol{v}_L,\boldsymbol{0}}e^{-\left(\frac{\beta}{2}+it\right)H}\Psi_{\boldsymbol{v}_R,\boldsymbol{0}}\right). \tag{4}$$

Here, for conciseness, we introduce the integer $n_{\boldsymbol{v}_L,\boldsymbol{v}_R} = (|\boldsymbol{v}_L| + 1)|\boldsymbol{v}_R|$. For chaotic systems, the Wightman function is expected to decay with time. On the other hand, at $t = \beta = 0$ we have $c_{\boldsymbol{v}_L,\boldsymbol{v}_R}(t) = i^{n_{\boldsymbol{v}_L,\boldsymbol{v}_R}}$ for $\boldsymbol{v}_L = \boldsymbol{v}_R$ and $c_{\boldsymbol{v}_L,\boldsymbol{v}_R}(t) = 0$ otherwise. It is therefore natural to focus on the contribution from $c_{\boldsymbol{v},\boldsymbol{v}}(t)$ in Eq. (3). Next, we classify operators $\Psi_{\boldsymbol{v},\boldsymbol{0}}$ into three categories [86]: (1) operators with small size $|\boldsymbol{v}|$, (2) operators with near-maximal size $|\boldsymbol{v}| \approx N$, and (3) complex operators with $|\boldsymbol{v}|, N - |\boldsymbol{v}| \sim O(N)$. Class (1) contains simple operators, for which the Wightman function is finite; however, the number of such operators is itself only $O(1)$. Operators in class (2) are analogous as they are obtained by multiplying class (1) operators by the fermion parity operator. By contrast, the overwhelming majority of operators belong to class (3). For chaotic systems with all-to-all interactions, these complex operators cannot be distinguished either by their locality structure or by their overlap with conserved charges. It is therefore natural to assume that their Majorana spectra are approximately uniform [47]. Therefore, we estimate their contribution by averaging over all choices of $\boldsymbol{v}$, leading to

$$\overline{(-i)^{n_{v,v}}c_{v,v}(t)} = \frac{1}{Z(\beta)2^{N/2}}\left|Z\left(\frac{\beta}{2}+it\right)\right|^2. \qquad (5)$$

Here, we isolate a phase factor. The SFF already appears. Neglecting the fluctuations of $c_{v_L,v_R}(t)$ around its expectation value and adding back contributions from simple operators, we find

$$\frac{1}{2^N}\sum_{v_L,v_R} c_{v_L,v_R}(t)^4 \approx C_0 2^{-N} + \frac{\mathrm{SFF}_{\beta/2}(t)^4}{2^{2N}Z(\beta)^4}. \qquad (6)$$

Here, $C_0 \sim O(1)$ is a constant. We expect that contributions from operators with $v_L \neq v_R$ only renormalize C_0, as estimated in Supplemental Material [87].

Equation (6) shows the expected behavior of magic growth. At $\beta = t = 0$, the second term becomes unity while the first term is negligible, leading to $M_2 = 0$. With this motivation, one may try dropping the first term:

$$M_2(t) \approx 2N\ln 2 - 4\ln[\mathrm{SFF}_{\beta/2}(t)/Z(\beta)] \equiv M_2^{(p)}(t). \qquad (7)$$

This provides a direct relation between the SRE and the SFF. Using the general features of the SFF, Eq. (7) predicts a nonmonotonic behavior of the SRE. In the slope regime of the SFF, the SRE increases and is self-averaging. This increase terminates when the dynamics enter the ramp regime, where the SRE decays logarithmically. Finally, the SRE saturates in the plateau regime. However, since $\mathrm{SFF}_{\beta/2}(\infty) = Z(\beta)$ in the plateau regime, Eq. (7) predicts $M_2(t) = 2N\ln 2$ in the long-time limit. This indicates that Eq. (7) already violates the bound $M_2(t) \leq N\ln 2$ in the slope regime at sufficiently long times. This violation is a close analog of the information paradox for the entanglement entropy [89], particularly for the dynamics of the thermofield double state [90,91]. Adding back the 2^{-N} term resolves this paradox and, in the thermodynamic limit, leads to

$$M_2(t) \approx \mathrm{Min}\{N\ln 2, M_2^{(p)}(t)\}. \qquad (8)$$

For high-temperature regimes, this results in a first-order dynamical transition at t_* (in the slope regime) determined by $N\ln 2 = M_2^{(p)}(t_*)$, resulting a singularity in the SRE. In the low-temperature limit, it is possible that $M_2^{(p)}(t) > N\ln 2$ for arbitrary times t, due to the extensive magic resources due to imaginary-time evolution.

The Sachdev-Ye-Kitaev model—To further demonstrate the validity of Eq. (8) in microscopic Hamiltonians without introducing Haar integrals, we study the dynamics of the SRE in the SYK model [80–83]. The model describes N randomly interacting Majorana fermion modes with Hamiltonian

$$H = \sum_{i_1<i_2<\cdots<i_q} i^{\frac{q(q-1)}{2}} J_{i_1 i_2\cdots i_q}\psi_{i_1}\psi_{i_2}\cdots\psi_{i_q}, \qquad (9)$$

where the random couplings $J_{i_1 i_2\cdots i_q}$ are independent Gaussian variables with

$$\overline{J_{i_1 i_2\cdots i_q}} = 0, \qquad \overline{J^2_{i_1 i_2\cdots i_q}} = (q-1)!J^2/N^{q-1}. \qquad (10)$$

The SYK model is chaotic for $q \geq 4$, exhibiting random-matrix behavior [56] and an emergent holography [81,82,92]. It also serves as a concrete solvable model for non-Fermi liquids [83]. Numerical studies of the SRE dynamics in the SYK model have been performed using exact diagonalization for finite N in Refs. [24–27].

We study the SRE dynamics of the SYK model in TFD states at $N \to \infty$ by employing the path-integral representation of $Z_{\mathrm{SRE}} = Z(\beta)^4 \sum_{v_L,v_R} c_{v_L,v_R}(t)^4$, as illustrated in Fig. 1. Four copies of the Majorana fermion fields $\psi_j^{(\alpha)}$, with $\alpha \in \{1,2,3,4\}$, arise from the four replicas of the density matrix (different colors in Fig. 1). The original definition of the SRE requires extensive operator insertions. Following the construction in Ref. [40], this can be equivalently formulated by introducing auxiliary Ising spins [87], which leads to [93]

$$Z_{\mathrm{SRE}} = \sum_{\sigma_{L/R,j}} \left\langle \prod_j \mathcal{S}^{(12,34)}_{j,it}[\sigma_{L,j}]\mathcal{S}^{(12,34)}_{j,\beta/2}[\sigma_{R,j}] \right\rangle_0, \qquad (11)$$

where $\sigma_{L/R,j} = \pm 1$ are $2N$ Ising variables. $\mathcal{S}^{(12,34)}_{j,\theta}[\sigma]$ is the fermionic SWAP (fSWAP) operation (with complex time $\theta = \tau + it$) that imposes

$$\psi_j^{(1)}(\theta^+) = -\sigma\psi_j^{(2)}(\theta^-), \quad \psi_j^{(2)}(\theta^+) = \sigma\psi_j^{(1)}(\theta^-), \qquad (12)$$

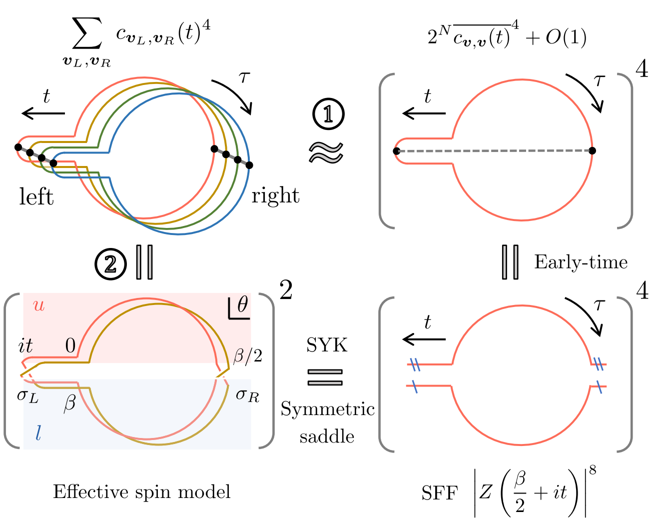

FIG. 1. Illustration of two independent approaches to relate the SRE to the SFF at early times, as elaborated in the main text. In method ①, we focus on $c_{v,v}(t)$ and approximate it by averaging over v. The early-time regime before saturation is dominated by the contribution from the SFF. In method ②, we focus on SYK-like models and assume that the Z_2 symmetry is preserved. In the long-time limit, saddles that break this symmetry can emerge.

and similarly for $(\psi_j^{(3)}, \psi_j^{(4)})$. We highlight that the effective spin model now exhibits a global Z_2 symmetry $(\sigma_{L/R,j}, \psi_j^{(2)}, \psi_j^{(4)}) \to -(\sigma_{L/R,j}, \psi_j^{(2)}, \psi_j^{(4)})$, which plays an central role in later discussions.

Because of the presence of two fSWAP operators for each pair of replicas, the upper branch (denoted as u) of one replica becomes connected to the lower branch (denoted as l) of the other replica, with an additional phase $\sigma_{L/R,j}$ acquired when passing through the connection point, as illustrated in Fig. 1. Therefore, it is convenient to define

$$\psi_j^{[1]}(\theta) \equiv \begin{cases} \psi_j^{(1)}(\theta) & \theta \in u \ (\mathrm{Re}\theta < \beta/2), \\ \psi_j^{(2)}(\theta) & \theta \in l \ (\mathrm{Re}\theta > \beta/2), \end{cases} \tag{13}$$

and similarly for other replicas. Then, $\psi_j^{[\alpha]}$ with different α becomes disconnected. For the SYK model, this implies that the two-point function $G^{[\alpha\gamma]}(\theta_1, \theta_2) = \langle \psi_j^{[\alpha]}(\theta_1)\psi_j^{[\gamma]}(\theta_2)\rangle = \delta^{\alpha\gamma} G(\theta_1, \theta_2)$ is diagonal in $\alpha\gamma$ [94]. As derived in Supplemental Material [87], Green's function satisfies the saddle-point equations:

$$\begin{aligned} \Sigma(\theta_1, \theta_2) &= J^2 f(\theta_1) f(\theta_2) G(\theta_1, \theta_2)^{q-1}, \\ G(\theta_1, \theta_2) &= \frac{\sum_\sigma g_\sigma(\theta_1, \theta_2)[\det g_\sigma]^{-2}}{\sum_\sigma [\det g_\sigma]^{-2}}. \end{aligned} \tag{14}$$

Here, we have introduced $f(\theta) = 1, i, -i$ when θ lies on the branch with imaginary, forward, or backward evolution, respectively [87,95]. The function $g_\sigma = (\partial_\tau - \Sigma)_\sigma^{-1}$ denotes Green's function evaluated with $\sigma_L = \sigma_R = \sigma$ for a representative site, where the u and l branches are joined with a phase σ at both ends. The SRE can then be computed using the saddle-point solutions [87].

We are now ready to demonstrate the relation between the SRE and the SFF in the SYK model. First, we assume that the Z_2 symmetry is unbroken. As a result, both $G(\theta_1, \theta_2)$ and $\Sigma(\theta_1, \theta_2)$ are nonzero only if θ_1 and θ_2 both lie on either the u or the l branch. The self-consistent equation can be equivalently written as

$$\Sigma(\theta_1, \theta_2) = J^2 P(\theta_1, \theta_2) f(\theta_1) f(\theta_2) g_\sigma(\theta_1, \theta_2)^{q-1}. \tag{15}$$

Here, $P(\theta_1, \theta_2) = 1$ if θ_1 and θ_2 both lie on the u or the l branch and vanishes otherwise. It also guarantees that the saddle-point solution of $\Sigma(\theta_1, \theta_2)$ is independent of σ. On the other hand, the same saddle-point equation shows up when evaluating

$$\tilde{Z} = \langle \mathrm{EPR}_{\boldsymbol{\sigma}} | e^{-\left(\frac{\beta}{2} - it\right) H} \otimes e^{-\left(\frac{\beta}{2} + it\right) \tilde{H}} | \mathrm{EPR}_{\boldsymbol{\sigma}} \rangle. \tag{16}$$

This inner product is again defined for a system containing $2N$ Majorana fermions, ψ_j and ξ_j. The vector $\boldsymbol{\sigma}$ is an N-dimensional vector that specifies the EPR state via $(\psi_j + i\sigma_j \xi_j)|\mathrm{EPR}_{\boldsymbol{\sigma}}\rangle = 0$. The Hamiltonian H is given by Eq. (9), while $\tilde{H}$ is obtained from H by (1) replacing ψ_j with ξ_j and (2) replacing $J_{i_1 i_2 \cdots i_q}$ with independently sampled couplings $\tilde{J}_{i_1 i_2 \cdots i_q}$. In particular, the presence of independent couplings guarantees the appearance of $P(\theta_1, \theta_2)$ in the saddle-point equations. Since the partition function of the SRE contains four replicas, we expect $Z_{\mathrm{SRE}} \propto \tilde{Z}^4$, up to factors that are independent of βJ and tJ. Finally, because $\tilde{Z}$ is independent of $\boldsymbol{\sigma}$, we can perform a summation over all $\boldsymbol{\sigma}$. Noting that the states $|\mathrm{EPR}_{\boldsymbol{\sigma}}\rangle$ with different $\boldsymbol{\sigma}$ form a complete basis, we find

$$\tilde{Z} \propto \mathrm{tr}\left[e^{-\left(\frac{\beta}{2} - it\right) H}\right] \times \mathrm{tr}\left[e^{-\left(\frac{\beta}{2} + it\right) \tilde{H}}\right] = \mathrm{SFF}_{\beta/2}(t)\Big|_{\mathrm{slope}}. \tag{17}$$

This relation between $\tilde{Z}$ and the SFF holds only when the SFF is dominated by the disconnected solution between the forward- and backward-evolution branches. This precisely corresponds to the self-averaged slope regime [57]. Using Eq. (17), we conclude that the relation proposed in Eq. (7) becomes *exact* for the symmetric saddle of the SRE and the slope regime of the SFF.

The discussion in the previous section indicates that the symmetric saddle is eventually replaced by a saddle exhibiting spontaneous symmetry breaking (SSB), which prevents the growth of the SRE beyond its upper bound. Here, we focus exclusively on the regime deep in the symmetry-breaking phase, where only $\sigma = 1$ contributes in Eq. (14) due to $\det g_1 \ll \det g_{-1}$. As a result, we can approximate $G(\theta_1, \theta_2) \approx g_1(\theta_1, \theta_2)$, and the saddle-point equation reduces to that of the conventional Keldysh contour, $Z(\beta) \approx \mathrm{tr}[e^{iHt} e^{-iHt} e^{-\beta H}]$ [96]. Accounting for the four replicas, we then obtain $Z_{\mathrm{SRE}} = Z(\beta)^4$, which yields $M_2(t) \approx N \ln 2$. Combined with the symmetric saddle, this yields the behavior in Eq. (8). Finally, we emphasize that, although the above discussion is illustrated using the original SYK model, the same conclusions apply to a large class of generalizations such as randomly coupled SYK models [97–100] or higher-dimensional SYK models [101,102].

Numerics—We now present results for the SRE obtained by numerically solving the saddle-point equations for $q = 4$. Similar methods have previously been applied to the study of the Rényi entropy of density matrices [91,95]. As shown in Figs. 2(a)–2(c), there exist multiple saddle-point solutions, which are plotted together with the order parameter $\langle \sigma \rangle$ for the Z_2 symmetry, defined as

$$\langle \sigma \rangle = \sum_\sigma \sigma [\det g_\sigma]^{-2} \Big/ \sum_\sigma [\det g_\sigma]^{-2}. \tag{18}$$

The saddle-point solution with $\langle \sigma \rangle = 0$ is symmetric, while the solution with $\langle \sigma \rangle \neq 0$ exhibits SSB. We have also numerically verified that the symmetric solution satisfies Eq. (7) to machine precision by independently computing the SFF in the slope regime.

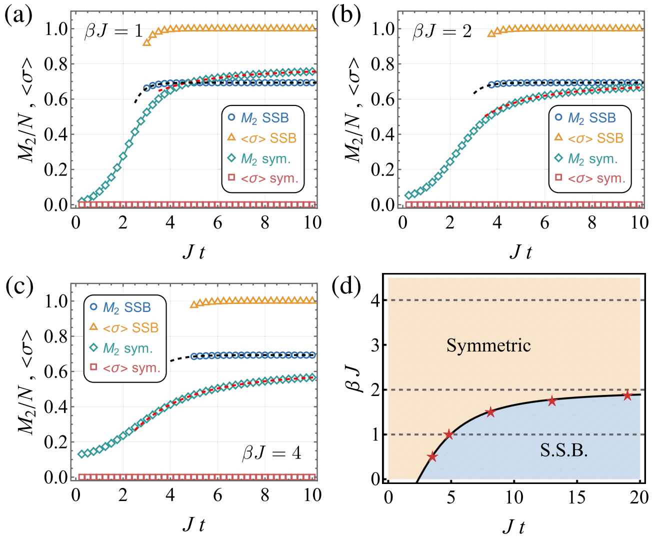

FIG. 2. Numerical results for the SRE in the SYK model with $q = 4$. (a)–(c) Time evolution of the SRE and the order parameter $\langle\sigma\rangle$ on different saddle points at different temperatures. The dashed lines represent fits, as described in the main text. (d) Phase diagram of the SRE. The phase boundary is obtained by fitting data points denoted by red stars [with an additional data point at (48.3,2)].

At high temperatures, $\beta J = 1$, the early-time SRE is dominated by the symmetric saddle, while the dynamical transition to the saddle with SSB occurs at $t_* J \approx 4.8$. The symmetry-breaking saddle is nearly fully polarized, leading to an almost maximal SRE. To further quantify the late-time behavior, we fit the numerical results on the SSB saddle using $M_2/N = \ln 2 - a_0 e^{-b_0 J t}$. The resulting fit, shown by the black dashed lines, matches the numerical data with high accuracy. When the temperature decreases, there are important modifications. First, the initial value $M_2(0)$ increases due to the imaginary-time evolution. The Eq. (7) predicts $M_2(0) = 2N \ln 2 - 4S^{(2)}(\beta/2)$, where $S^{(2)}(\beta)$ is the second Rényi entropy of the thermal density matrix. For the SYK model, $S^{(2)}(\infty) = 0.2324$ [82]. As a result, we always have $M_2(0) < N \ln 2$. Second, the growth of the symmetric solution becomes significantly slower and does not exhibit a transition to the SSB saddle at finite t for $\beta J \gtrsim 2$. We expect that this behavior stems from the soft reparametrization mode in the SYK model, which similarly slows entanglement dynamics [84,103]. These reparametrization modes are governed by the Schwarzian action [82], which admits an exact partition function $Z_{\mathrm{sch}}(\beta) \propto \beta^{-3/2} \exp(2\pi^2 C/\beta J)$ with $C \propto N$ [104]. In the slope regime, the SFF can be obtained by the analytical continuation of Z_{sch}, which leads to

$$M_2^{(p)}(t) = M_2(0) + \frac{32\pi^2 C}{\beta J} \frac{4t^2}{\beta^2 + 4t^2} + 6 \ln\left(\frac{\beta^2 + 4t^2}{\beta^2}\right). \tag{19}$$

The saddle-point analysis reproduces only the first two terms, which are extensive in N. Consequently, we obtain $M_2(\infty) - M_2(0) = (32\pi^2 C/\beta J)$, which decreases as βJ increases, consistent with the numerical observations. Further numerical evidence for the relevance of soft modes is provided in Supplemental Material [87]. Motivated by this analysis, we further fit the numerical results for the symmetric saddle using $M_2/N = a_0 + (b_0/c_0 + J^2 t^2)$. The resulting fits, shown by the red dashed lines, match the numerical data at long times with good accuracy even for $\beta J = 1$. The analysis also indicates that, at exponential long times before the dip time, $t \sim e^N \lesssim t_{\mathrm{dip}}$, the last term in Eq. (19) yields $M_2^{(p)}(t) > N \ln 2$, at which point a transition to the symmetry-breaking saddle occurs. Finally, we present a phase diagram for the SRE in Fig. 2(d), where the phase boundary is determined by fitting the numerical data with $\beta J = a_0 + (b_0/c_0 + J^2 t_*^2)$.

Discussions—In this Letter, we establish a connection between the SRE dynamics of TFD states and the SFF through both a general argument and a concrete study of the SYK model. Our results reveal a dynamical transition between an early-time regime, captured by the slope regime of the SFF, and a late-time regime with a nearly maximal SRE. In the SYK model, these distinct regimes are described by different saddle points in the path-integral representation, where an emergent $\mathbb{Z}_2$ symmetry plays a pivotal role. At low temperatures, soft reparametrization modes delay this transition to exponentially long times. Our findings provide a universal link between spectral statistics and the emergence of classical simulation hardness, shedding new light on the growth of quantum complexity and resources.

In Supplemental Material [87], we provide additional results that highlight the generality of the relation between the SRE and the SFF, including exact diagonalization studies of quantum spin models with and without spatial locality, as well as a generalization of the relation to arbitrary stabilizer initial states in generic systems in the short-time limit. There are many interesting directions for future research. For example, performing larger-scale numerical studies of many-body systems is of particular interest. One promising candidate, closely related to holography, is the hyperbolic Ising model [105,106], which shares the maximally chaotic features of the SYK model. Investigating how magic resources are connected to other measures of quantum chaos, such as out-of-time-order correlators [81,107] and Krylov complexity [108–110], may uncover richer structures and provide a more unified perspective on chaotic quantum dynamics. We leave these directions for future work.

Acknowledgments—We thank Hanteng Wang, Zhi-Cheng Yang, Tian-Gang Zhou, and Yi-Neng Zhou for helpful discussions. This project is supported by the Shanghai Rising-Star Program under Grant

No. 24QA2700300, the NSFC under Grant No. 12374477, the Quantum Science and Technology-National Science and Technology Major Project No. 2024ZD0300101, and the Xuemin Institute of Advanced Studies, Fudan University.

Data availability—The data that support the findings of this article are openly available [111]; embargo periods may apply.

[1] S. R. White, Density matrix formulation for quantum renormalization groups, Phys. Rev. Lett. **69**, 2863 (1992).
[2] R. Orús, Tensor networks for complex quantum systems, Nat. Rev. Phys. **1**, 538 (2019).
[3] M. A. Nielsen and I. L. Chuang, *Quantum Computation and Quantum Information* (Cambridge University Press, Cambridge, England, 2010).
[4] D. Gottesman, Stabilizer codes and quantum error correction, arXiv:quant-ph/9705052.
[5] D. Gottesman, The Heisenberg representation of quantum computers, in 22nd International Colloquium on Group Theoretical Methods in Physics (1998), pp. 32–43, arXiv:quant-ph/9807006.
[6] D. Gottesman, Theory of fault-tolerant quantum computation, Phys. Rev. A **57**, 127 (1998).
[7] S. Aaronson and D. Gottesman, Improved simulation of stabilizer circuits, Phys. Rev. A **70**, 052328 (2004).
[8] L. Leone, S. F. E. Oliviero, and A. Hamma, Stabilizer Rényi entropy, Phys. Rev. Lett. **128**, 050402 (2022).
[9] T. Haug and L. Piroli, Stabilizer entropies and nonstabilizerness monotones, Quantum **7**, 1092 (2023).
[10] Y. Wang and Y. Li, Stabilizer Rényi entropy on qudits, Quantum Inf. Process. **22**, 444 (2023).
[11] X. Huang, H.-Z. Li, and J.-X. Zhong, A fast and exact algorithm for stabilizer Rényi entropy via XOR-FWHT, arXiv:2512.24685.
[12] Z. Xiao and S. Ryu, Exponentially accelerated sampling of Pauli strings for nonstabilizerness, arXiv:2601.00761.
[13] P. Sierant, J. Vallès-Muns, and A. Garcia-Saez, Computing quantum magic of state vectors, Quantum **10**, 2059 (2026).
[14] M. Howard and E. Campbell, Application of a resource theory for magic states to fault-tolerant quantum computing, Phys. Rev. Lett. **118**, 090501 (2017).
[15] Z.-W. Liu and A. Winter, Many-body quantum magic, PRX Quantum **3**, 020333 (2022).
[16] M. Beverland, E. Campbell, M. Howard, and V. Kliuchnikov, Lower bounds on the non-Clifford resources for quantum computations, Quantum Sci. Technol. **5**, 035009 (2020).
[17] E. Tirrito, P. S. Tarabunga, G. Lami, T. Chanda, L. Leone, S. F. E. Oliviero, M. Dalmonte, M. Collura, and A. Hamma, Quantifying nonstabilizerness through entanglement spectrum flatness, Phys. Rev. A **109**, L040401 (2024).
[18] X. Turkeshi, M. Schirò, and P. Sierant, Measuring nonstabilizerness via multifractal flatness, Phys. Rev. A **108**, 042408 (2023).
[19] A. Paviglianiti, G. Lami, M. Collura, and A. Silva, Estimating nonstabilizerness dynamics without simulating it, PRX Quantum **6**, 030320 (2025).
[20] A. Ahmadi and E. Greplova, Quantifying non-stabilizerness via information scrambling, SciPost Phys. **16**, 043 (2024).
[21] D. Qian and J. Wang, Quantum nonlocal nonstabilizerness, Phys. Rev. A **111**, 052443 (2025).
[22] C. D. White, C. Cao, and B. Swingle, Conformal field theories are magical, Phys. Rev. B **103**, 075145 (2021).
[23] R. Smith, Z. Papić, and A. Hallam, Nonstabilizerness in kinetically constrained Rydberg atom arrays, Phys. Rev. B **111**, 245148 (2025).
[24] S. Bera and M. Schirò, Non-stabilizerness of Sachdev-Ye-Kitaev model, SciPost Phys. **19**, 159 (2025).
[25] B. Jasser, J. Odavic, and A. Hamma, Stabilizer entropy and entanglement complexity in the Sachdev-Ye-Kitaev model, Phys. Rev. B **112**, 174204 (2025).
[26] A. Russomanno, G. Passarelli, D. Rossini, and P. Lucignano, Nonstabilizerness in the unitary and monitored quantum dynamics of XXZ-staggered and Sachdev-Ye-Kitaev models, Phys. Rev. B **112**, 064312 (2025).
[27] V. Malvimat, M. Sarkis, Y. Suk, and J. Yoon, Multipartite non-local magic and SYK model, arXiv:2601.03076.
[28] J. Odavić, M. Viscardi, and A. Hamma, Stabilizer entropy in nonintegrable quantum evolutions, Phys. Rev. B **112**, 104301 (2025).
[29] G. Passarelli, R. Fazio, and P. Lucignano, Nonstabilizerness of permutationally invariant systems, Phys. Rev. A **110**, 022436 (2024).
[30] P. S. Tarabunga and C. Castelnovo, Magic in generalized Rokhsar-Kivelson wavefunctions, Quantum **8**, 1347 (2024).
[31] P. S. Tarabunga, Critical behaviors of non-stabilizerness in quantum spin chains, Quantum **8**, 1413 (2024).
[32] A. G. Catalano, J. Odavić, G. Torre, A. Hamma, F. Franchini, and S. M. Giampaolo, Magic phase transition and non-local complexity in generalized W state, SciPost Phys. Core **8**, 078 (2025).
[33] M. Viscardi, M. Dalmonte, A. Hamma, and E. Tirrito, Interplay of entanglement structures and stabilizer entropy in spin models, SciPost Phys. Core **9**, 012 (2026).
[34] Y.-M. Ding, Z. Wang, and Z. Yan, Evaluating many-body stabilizer Rényi entropy by sampling reduced Pauli strings: Singularities, volume law, and nonlocal magic, PRX Quantum **6**, 030328 (2025).
[35] P. S. Tarabunga, E. Tirrito, T. Chanda, and M. Dalmonte, Many-body magic via Pauli-Markov chains—From criticality to gauge theories, PRX Quantum **4**, 040317 (2023).
[36] S. F. E. Oliviero, L. Leone, and A. Hamma, Magic-state resource theory for the ground state of the transverse-field Ising model, Phys. Rev. A **106**, 042426 (2022).
[37] M. Collura, J. De Nardis, V. Alba, and G. Lami, The quantum magic of fermionic Gaussian states, Quantum **10**, 2036 (2026).
[38] C. Wang, Z.-C. Yang, T. Zhou, and X. Chen, Magic transition in monitored free fermion dynamics, arXiv:2507.10688.
[39] H.-Z. Li, Y.-R. Zhang, Y.-J. Zhao, X. Huang, and J.-X. Zhong, Nonstabilizerness in Stark many-body localization, Phys. Rev. B **113**, 104305 (2026).

[40] P. Zhang, S. Zhou, and N. Sun, Stabilizer Rényi entropy and its transition in the coupled Sachdev-Ye-Kitaev model, Phys. Rev. Lett. **136**, 080201 (2026).

[41] J. Q. Fang, F.-H. Wang, and X. Y. Xu, Two-point stabilizer Rényi entropy: A computable magic proxy of interacting fermions, arXiv:2601.13314.

[42] D. Rattacaso, L. Leone, S. F. E. Oliviero, and A. Hamma, Stabilizer entropy dynamics after a quantum quench, Phys. Rev. A **108**, 042407 (2023).

[43] G. Lami and M. Collura, Nonstabilizerness via perfect Pauli sampling of matrix product states, Phys. Rev. Lett. **131**, 180401 (2023).

[44] T. Haug and L. Piroli, Quantifying nonstabilizerness of matrix product states, Phys. Rev. B **107**, 035148 (2023).

[45] G. Lami and M. Collura, Unveiling the stabilizer group of a matrix product state, Phys. Rev. Lett. **133**, 010602 (2024).

[46] P. S. Tarabunga and T. Haug, Efficient mutual magic and magic capacity with matrix product states, SciPost Phys. **19**, 085 (2025).

[47] X. Turkeshi, A. Dymarsky, and P. Sierant, Pauli spectrum and nonstabilizerness of typical quantum many-body states, Phys. Rev. B **111**, 054301 (2025).

[48] Y. Zhang and Y. Gu, Quantum magic dynamics in random circuits, npj Quantum Inf. **12**, 87 (2026).

[49] X. Turkeshi, E. Tirrito, and P. Sierant, Magic spreading in random quantum circuits, Nat. Commun. **16**, 2575 (2025).

[50] E. Tirrito, X. Turkeshi, and P. Sierant, Anticoncentration and magic spreading under ergodic quantum dynamics, Phys. Rev. Lett. **135**, 220401 (2025).

[51] T. Haug, L. Aolita, and M. S. Kim, Probing quantum complexity via universal saturation of stabilizer entropies, Quantum **9**, 1801 (2025).

[52] D. Szombathy, A. Valli, C. P. Moca, J. Asbóth, L. Farkas, T. Rakovszky, and G. Zaránd, Spectral properties versus magic generation in T-doped random Clifford circuits, Phys. Rev. Res. **7**, 043080 (2025).

[53] D. Szombathy, A. Valli, C. P. Moca, L. Farkas, and G. Zaránd, Independent stabilizer Rényi entropy and entanglement fluctuations in random unitary circuits, Phys. Rev. Res. **7**, 043072 (2025).

[54] Z.-Y. Hou, C. Cao, and Z.-C. Yang, Stabilizer entanglement enhances magic injection, arXiv:2503.20873.

[55] M. L. Mehta, *Random Matrices* (Elsevier, New York, 2004), Vol. 142.

[56] J. S. Cotler, G. Gur-Ari, M. Hanada, J. Polchinski, P. Saad, S. H. Shenker, D. Stanford, A. Streicher, and M. Tezuka, Black holes and random matrices, J. High Energy Phys. 05 (2017) 118; 09 (2018) 002(E).

[57] P. Saad, S. H. Shenker, and D. Stanford, A semiclassical ramp in SYK and in gravity, arXiv:1806.06840.

[58] J. M. Deutsch, Quantum statistical mechanics in a closed system, Phys. Rev. A **43**, 2046 (1991).

[59] M. Srednicki, The approach to thermal equilibrium in quantized chaotic systems, J. Phys. A **32**, 1163 (1999).

[60] M. Rigol, V. Dunjko, and M. Olshanii, Thermalization and its mechanism for generic isolated quantum systems, Nature (London) **452**, 854 (2008).

[61] A. M. Kaufman, M. E. Tai, A. Lukin, M. Rispoli, R. Schittko, P. M. Preiss, and M. Greiner, Quantum thermalization through entanglement in an isolated many-body system, Science **353**, aaf6725 (2016).

[62] M. Khramtsov and E. Lanina, Spectral form factor in the double-scaled SYK model, J. High Energy Phys. 03 (2020) 031.

[63] W. Israel, Thermo field dynamics of black holes, Phys. Lett. A **57**, 107 (1976).

[64] J. M. Maldacena, Eternal black holes in anti-de Sitter, J. High Energy Phys. 04 (2003) 021.

[65] Z. Liu, L. Chen, Y. Zhang, S. Zhou, and P. Zhang, Diagnosing strong-to-weak symmetry breaking via Wightman correlators, Commun. Phys. **8**, 274 (2025).

[66] Z. Weinstein, Efficient detection of strong-to-weak spontaneous symmetry breaking via the Rényi-1 correlator, Phys. Rev. Lett. **134**, 150405 (2025).

[67] P. Gao, D. L. Jafferis, and A. C. Wall, Traversable wormholes via a double trace deformation, J. High Energy Phys. 12 (2016) 151.

[68] J. Maldacena, D. Stanford, and Z. Yang, Diving into traversable wormholes, Fortschr. Phys. **65**, 1700034 (2017).

[69] L. Susskind and Y. Zhao, Teleportation through the wormhole, Phys. Rev. D **98**, 046016 (2018).

[70] P. Gao and H. Liu, Regenesis and quantum traversable wormholes, J. High Energy Phys. 10 (2018) 048.

[71] A. R. Brown, H. Gharibyan, S. Leichenauer, H. W. Lin, S. Nezami, G. Salton, L. Susskind, B. Swingle, and M. Walter, Quantum gravity in the lab. I. Teleportation by size and traversable wormholes, PRX Quantum **4**, 010320 (2023).

[72] P. Gao and D. L. Jafferis, A traversable wormhole teleportation protocol in the SYK model, J. High Energy Phys. 07 (2019) 097.

[73] T. Schuster, B. Kobrin, P. Gao, I. Cong, E. T. Khabiboulline, N. M. Linke, M. D. Lukin, C. Monroe, B. Yoshida, and N. Y. Yao, Many-body quantum teleportation via operator spreading in the traversable wormhole protocol, Phys. Rev. X **12**, 031013 (2022).

[74] D. Jafferis, A. Zlokapa, J. D. Lykken, D. K. Kolchmeyer, S. I. Davis, N. Lauk, H. Neven, and M. Spiropulu, Traversable wormhole dynamics on a quantum processor, Nature (London) **612**, 51 (2022); **640**, E32 (2025).

[75] S. Zhou, P. Zhang, and Z. Yu, Environment-induced transitions in many-body quantum teleportation, Phys. Rev. Res. **8**, L012007 (2026).

[76] Z. Liu and P. Zhang, Fidelity of wormhole teleportation in finite-qubit systems, J. High Energy Phys. 07 (2024) 031.

[77] C. Burrage, C. Käding, P. Millington, and J. Minář, Open quantum dynamics induced by light scalar fields, Phys. Rev. D **100**, 076003 (2019).

[78] C. Käding and M. Pitschmann, New method for directly computing reduced density matrices, Phys. Rev. D **107**, 016005 (2023).

[79] C. Käding and M. Pitschmann, Density matrices in quantum field theory: Non-Markovianity, path integrals and master equations, arXiv:2503.08567.

[80] S. Sachdev and J. Ye, Gapless spin fluid ground state in a random, quantum Heisenberg magnet, Phys. Rev. Lett. **70**, 3339 (1993).

[81] A. Kitaev, in Talk Given at Fundamental Physics Prize Symposium (2014), http://online.kitp.ucsb.edu/online/joint98/.

[82] J. Maldacena and D. Stanford, Remarks on the Sachdev-Ye-Kitaev model, Phys. Rev. D **94**, 106002 (2016).

[83] D. Chowdhury, A. Georges, O. Parcollet, and S. Sachdev, Sachdev-ye-Kitaev models and beyond: Window into non-Fermi liquids, Rev. Mod. Phys. **94**, 035004 (2022).

[84] Y. Gu, A. Lucas, and X.-L. Qi, Spread of entanglement in a Sachdev-Ye-Kitaev chain, J. High Energy Phys. 09 (2017) 120.

[85] M.-D. Choi, Completely positive linear maps on complex matrices, Linear Algebra Appl. **10**, 285 (1975).

[86] This simple classification neglects the locality structure of the model and is therefore expected to be valid for systems with all-to-all interactions.

[87] See Supplementary Material at http://link.aps.org/supplemental/10.1103/p4s9-9smn for (1) an estimate of the contribution from operators with $\boldsymbol{v}_L \neq \boldsymbol{v}_R$, (2) a review of the representation of the SRE with auxiliary Ising spins, (3) the derivation of the self-consistent equation for the SRE in the SYK model, (4) numerical results with SYK_2 or SYK_6 perturbations, and (5) numerical study of the relation between the SRE and the SFF in quantum spin models, which also includes Ref. [88].

[88] H. Wang, C. Liu, P. Zhang, and A. M. García-García, Entanglement transition and replica wormholes in the dissipative Sachdev-Ye-Kitaev model, Phys. Rev. D **109**, 046005 (2024).

[89] S. W. Hawking, Breakdown of predictability in gravitational collapse, Phys. Rev. D **14**, 2460 (1976).

[90] A. Almheiri, R. Mahajan, and J. Maldacena, Islands outside the horizon, arXiv:1910.11077.

[91] Y. Chen, X.-L. Qi, and P. Zhang, Replica wormhole and information retrieval in the SYK model coupled to Majorana chains, J. High Energy Phys. 06 (2020) 121.

[92] J. Maldacena, D. Stanford, and Z. Yang, Conformal symmetry and its breaking in two dimensional nearly anti-de-Sitter space, Prog. Theor. Exp. Phys. **2016**, 12C104 (2016).

[93] Here, we make the disorder-replica-diagonal assumption to approximate the quenched average by the annealed average for the SRE, which is expected to be valid in the limit $N \to \infty$ [94].

[94] A. Kitaev and S. J. Suh, The soft mode in the Sachdev-Ye-Kitaev model and its gravity dual, J. High Energy Phys. 05 (2017) 183.

[95] P. Zhang, C. Liu, and X. Chen, Subsystem Rényi entropy of thermal ensembles for SYK-like models, SciPost Phys. **8**, 094 (2020).

[96] A. Kamenev, *Field Theory of Non-Equilibrium Systems* (Cambridge University Press, Cambridge, England, 2023).

[97] S. Banerjee and E. Altman, Solvable model for a dynamical quantum phase transition from fast to slow scrambling, Phys. Rev. B **95**, 134302 (2017).

[98] X. Chen, R. Fan, Y. Chen, H. Zhai, and P. Zhang, Competition between chaotic and nonchaotic phases in a quadratically coupled Sachdev-Ye-Kitaev model, Phys. Rev. Lett. **119**, 207603 (2017).

[99] X.-Y. Song, C.-M. Jian, and L. Balents, Strongly correlated metal built from Sachdev-ye-Kitaev models, Phys. Rev. Lett. **119**, 216601 (2017).

[100] S.-K. Jian and H. Yao, Solvable Sachdev-Ye-Kitaev models in higher dimensions: From diffusion to many-body localization, Phys. Rev. Lett. **119**, 206602 (2017).

[101] Y. Gu, X.-L. Qi, and D. Stanford, Local criticality, diffusion and chaos in generalized Sachdev-Ye-Kitaev models, J. High Energy Phys. 05 (2016) 125.

[102] R. A. Davison, W. Fu, A. Georges, Y. Gu, K. Jensen, and S. Sachdev, Thermoelectric transport in disordered metals without quasiparticles: The Sachdev-ye-Kitaev models and holography, Phys. Rev. B **95**, 155131 (2017).

[103] R. Sohal, L. Nie, X.-Q. Sun, and E. Fradkin, Thermalization of randomly coupled SYK models, J. Stat. Mech. (2022) 013103.

[104] D. Stanford and E. Witten, Fermionic localization of the Schwarzian theory, J. High Energy Phys. 10 (2017) 008.

[105] M. Asaduzzaman, S. Catterall, Y. Meurice, and G. C. Toga, Quantum Ising model on two-dimensional anti–de Sitter space, Phys. Rev. D **109**, 054513 (2024).

[106] G. C. Toga, A. Samlodia, and A. F. Kemper, Fast scrambling in the hyperbolic Ising model, arXiv:2503.00114.

[107] A. I. Larkin and Y. N. Ovchinnikov, Quasiclassical method in the theory of superconductivity, J. Exp. Theor. Phys. (1969), https://jetp.ras.ru/cgi-bin/e/index/e/28/6/p1200?a=list.

[108] D. E. Parker, X. Cao, A. Avdoshkin, T. Scaffidi, and E. Altman, A universal operator growth hypothesis, Phys. Rev. X **9**, 041017 (2019).

[109] P. Nandy, A. S. Matsoukas-Roubeas, P. Martínez-Azcona, A. Dymarsky, and A. del Campo, Quantum dynamics in Krylov space: Methods and applications, Phys. Rep. **1125–1128**, 1 (2025).

[110] E. Rabinovici, A. Sánchez-Garrido, R. Shir, and J. Sonner, Krylov complexity, arXiv:2507.06286.

[111] N. Sun, GitHub, https://github.com/atom-sun/MagicDynamics (2026).